

Domain Adaptation and Image Classification via Deep Conditional Adaptation Network

Pengfei Ge, Chuan-Xian Ren, Dao-Qing Dai, Hong Yan *Fellow, IEEE*

Abstract—Unsupervised domain adaptation aims to generalize the supervised model trained on a source domain to an unlabeled target domain. Marginal distribution alignment of feature spaces is widely used to reduce the domain discrepancy between the source and target domains. However, it assumes that the source and target domains share the same label distribution, which limits their application scope. In this paper, we consider a more general application scenario where the label distributions of the source and target domains are not the same. In this scenario, marginal distribution alignment-based methods will be vulnerable to negative transfer. To address this issue, we propose a novel unsupervised domain adaptation method, Deep Conditional Adaptation Network (DCAN), based on conditional distribution alignment of feature spaces. To be specific, we reduce the domain discrepancy by minimizing the Conditional Maximum Mean Discrepancy between the conditional distributions of deep features on the source and target domains, and extract the discriminant information from target domain by maximizing the mutual information between samples and the prediction labels. In addition, DCAN can be used to address a special scenario, Partial unsupervised domain adaptation, where the target domain category is a subset of the source domain category. Experiments on both unsupervised domain adaptation and Partial unsupervised domain adaptation show that DCAN achieves superior classification performance over state-of-the-art methods. In particular, DCAN achieves great improvement in the tasks with large difference in label distributions (6.1% on SVHN→MNIST, 5.4% in UDA tasks on Office-Home and 4.5% in Partial UDA tasks on Office-Home).

Index Terms—Domain adaptation, Image classification, Maximum mean discrepancy, Conditional distribution discrepancy, Mutual information.

I. INTRODUCTION

DEEP Convolutional Neural Networks (CNNs) have achieved great success in a variety of computer vision and machine learning applications [1]–[3]. A number of recent results show that when the deep networks are trained in large-scale datasets, the features show good generalization performance over a wide range of datasets and computer vision tasks [4], [5]. However, due to the dataset bias problem, test errors of these deep classification networks are large when the training set and test set have a significant gap in data distributions. Fine-tuning provides a straightforward way to

reduce feature bias on deep networks [6]. Unfortunately, fine-tuning deep network parameters in a new dataset requires a significant amount of labeled data, which are not available in many scenarios. Therefore, it is necessary and important to design algorithms that can transfer discrimination features from a labeled source domain to another related but unlabeled domain.

To address this problem, a more practical task called unsupervised domain adaptation (UDA) has been studied recently. UDA learns a classifier for the unlabeled target domain by transferring knowledge from a labeled source domain [7], [8]. Previous UDA methods are mainly based on shallow models [8]–[13], which are roughly divided into two categories, i.e., instance-based methods and feature-based methods. Instance-based adaptation methods [8], [9] reweigh samples in the source domain to better represent the target domain distribution, while feature-based methods [10]–[13] attempt to learn a shared and invariant feature space. However, limited by the model’s representation capacity, the performance of these methods does not exceed the deep UDA approach.

In recent years, with the development of deep neural networks, more robust models have been proposed to deal with UDA tasks [14]–[20]. These methods can be roughly classified into two categories: pixel-level methods and feature-level methods. Pixel-level methods [18]–[20] utilize deep generative models, such as generative adversarial network (GAN) [21], to learn a mapping function between the source and target domains. Thus they can transfer the supervised model on the source domain to the target domain. Feature-level methods [14]–[17] follow the idea that domain discrepancy becomes smaller in the deep feature space [4], [5], thus domain adaptation can be done by matching the deep features of the source and target domains. Let Z represent the features obtained by a deep network. To project data from different domains to a shared deep feature space, existing methods often rely on marginal distribution alignment, which reduces the discrepancy between $P^s(Z)$ and $P^t(Z)$. A common strategy is to minimize the maximum mean discrepancy (MMD) [22] or introduce the adversarial training [16], [23]. In addition, some methods use an extra entropy regularization to extract discriminant information in the target domain for better transfer performance [15], [24].

Deep UDA methods have achieved great success in many computer vision applications, but they are still challenged by the following issues. 1) Pixel-level methods focus on generating real images and therefore cannot fully leverage the representative power of supervised CNNs. 2) Marginal distribution alignment-based methods may suffer negative

P.F. Ge, C.X. Ren, and D.Q. Dai are with the Intelligent Data Center, School of Mathematics, Sun Yat-Sen University, Guangzhou, China.

H. Yan is with the Department of Electrical Engineering, City University of Hong Kong, Hong Kong.

This work is supported in part by the National Natural Science Foundation of China under Grants 61976229, 61906046, 61572536, 11631015, U1611265, in part by the Science and Technology Program of Guangzhou under Grant 201804010248, and in part by City University of Hong Kong (Project 9610460).

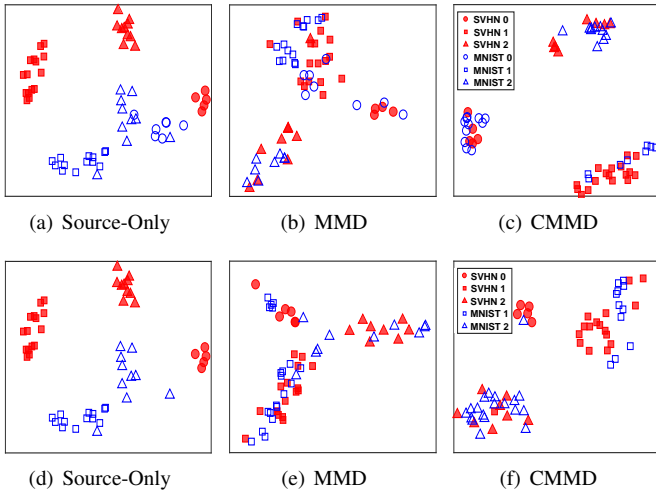


Fig. 1. Feature visualization with different methods on the task SVHN \rightarrow MNIST. Solid and hollow points represent the sample features of the source and target domains, respectively. Top: UDA task; Down: Partial UDA task. In particular, the target domain contains only two classes in the Partial UDA setting. (a) Visualization with the Source-Only model. (b) The results of aligning $P^s(Z)$ and $P^t(Z)$ by MMD. There is negative transfer between the source and target domains, and some samples of digit 0 in the target domain are incorrectly aligned. (c) The results of aligning $P^s(Z|Y)$ and $P^t(Z|Y)$ using CMMD. The categories in the target domain are correctly aligned with those in the source domain. (d)~(f) correspond to the Partial UDA setting, and similar results to UDA are obtained.

transfer resulting from the label distribution differences between source and target domains. In real-life scenarios, the label distributions of source and target domains are generally different. For example, on the UDA task SVHN \rightarrow MNIST, the number of digit 0 in SVHN is much less than that of 1 or 2, while these three classes are balanced in MNIST [25]. The visualization results with different methods are shown in Figure 1. In Figure 1(b), the marginal distribution alignment of feature spaces causes a portion of digit 0 in the target domain to be incorrectly matched to digit 1 in the source domain, thereby suffer from negative transfer. The Partial UDA task studied by recent literature [26], [27] also has this dilemma. In Figure 1(e), the marginal distribution alignment-based method leads to a more serious negative transfer problem in Partial UDA tasks. Therefore, marginal distribution alignment-based methods cannot deal with (Partial) UDA problems well. 3) The entropy regularization ignores the overall discriminant information, instead, only considers the discriminant information of a single sample. This manner makes the training process very unstable and may cause model degradation.

In order to tackle these challenges, we propose a new feature-level domain adaptation method, named Deep Conditional Adaptation Network (DCAN), which can align effectively the conditional distributions and extract discriminant information from the source and target domains. We first project the conditional distributions of features to the Reproducing Kernel Hilbert Space (RKHS) [28] with a nonlinear kernel function, and then use Conditional Maximum Mean Discrepancy (CMMD) [29] to measure the discrepancy between conditional distributions of source and target domains. The conditional distribution alignment with CMMD uses label

information to learn the conditional domain-invariant features, thus can be used to reduce the domain discrepancy and mitigate negative transfer, as shown in Figure 1(c) and Figure 1(f). In addition, we introduce mutual information to measure how much information is represented by the predicted category. By maximizing the mutual information between predicted category and sample on the target domain, we can extract the discriminant features effectively on the target domain. This mechanism helps us to transfer the classifier on the source domain to the target domain. DCAN does not enforce that the source and target domains share the same label distribution, thus it can also be used to deal with Partial UDA. We evaluate DCAN on four commonly used UDA benchmarks, i.e., Digit Datasets, Office-31, ImageCLEF-DA and Office-Home. We also evaluate DCAN under Partial setting on the Office-31 and Office-Home datasets for demonstration. The experiment results show that DCAN achieves state-of-the-art performance in all these tasks.

Our contributions are summarized as follows.

- 1) We propose a new deep domain adaptation approach, DCAN, to address both UDA and Partial UDA problems. DCAN can be trained in an end-to-end manner.
- 2) We introduce CMMD metric to match the conditional distributions of source and target domains, rather than the marginal distributions, thus DCAN alleviates the negative transfer problem. Mutual information is used to extract the discriminant information on target domain.
- 3) Extensive experiment results show that DCAN outperforms state-of-the-art UDA and Partial UDA methods on several image benchmarks. In particular, the average accuracy of three commonly used UDA tasks on digit datasets increases by 5.1%, the average accuracy of 12 UDA tasks on Office-Home increases by 5.4%. The average accuracy of 12 Partial UDA tasks on Office-Home increases by 4.5%.

The rest of this paper is organized as follows. Section II briefly reviews closely related works. In Section III, we introduce DCAN in detail. Two algorithms dealing with both UDA and Partial UDA problems are presented. In Section IV, experiment results and analysis are presented, and DCAN is compared with several state-of-the-art methods. Section V concludes this paper.

II. RELATED WORKS

In this section, we briefly review the visual domain adaption techniques from two directions, i.e., UDA and Partial UDA. Some preliminary of CMMD is also presented.

A. Unsupervised Domain Adaptation

MMD is the most common statistic used to measure domain discrepancy. Deep Domain Confusion (DDC) [14] combines the classification loss with a MMD-based domain confusion loss to learn a domain-invariant feature space. Deep Adaptation Networks (DAN) [15] use MMD of all task-specific layers to reduce domain discrepancy, and it achieves more robust results than DDC. Joint Adaptation Networks (JAN) [30] extends this idea by using joint maximum mean discrepancy to

match the joint distributions of the source and target domains. Residual transfer network (RTN) [17] introduces additional residual structures and entropy minimization to implement classifier adaptation. These methods need to align the marginal distributions, thus may suffer negative transfer resulting from the label distribution differences between source and target domains. Recently, this problem has received more attention. Weighted Domain Adaptation Network (WDAN) [25] proposes a weighted MMD to align feature distributions. It reweights the samples in source domain to eliminate class weight bias across domains. Balanced Distribution Adaptation (BDA) [31] simultaneously aligns the marginal and conditional distributions between domains to deal with the class imbalance issue in UDA. There are several major differences between our DCAN and these methods. 1) Compared with WDAN, DCAN also uses the discriminant information contained in the target domain when aligning feature distributions, but does not need to calculate the weight. 2) BDA uses the sum of MMD on each class to estimate the conditional distribution divergence, while DCAN introduces CMMD to directly estimate the conditional distribution divergence. 3) BDA requires a separate feature extraction process, while DCAN learns representative features in an end-to-end manner.

GAN is another common method for measuring domain discrepancy. Domain adversarial neural network (DANN) [16] introduces a domain discriminator to classify features of the source and target domains, while the feature extraction network learns domain-invariant features as much as possible to confuse the domain discriminator. Adversarial Discrimination Domain Adaptation (ADDA) [23] extends this idea by using different networks to extract the source and target features respectively. Conditional Domain Adversarial Network (CDAN) [32] trains a conditional generative adversarial network by the discrimination information conveyed in the classifier.

Heterogeneous domain adaptation (HDA) is another problem in the UDA literature, as multiple attributes, such as modalities, distributions and dimensions of data, are different across domains. Regularized Semi-Paired Kernel Canonical Correlation Analysis (RSP-KCCA) [33] introduces the KCCA to learn a domain-invariant feature space and proposes an effective optimization algorithm. Cross-domain neural-kernel networks (CNKN) [34] proposes the neural-kernel networks consisting of two coupled stream neural networks and a Fourier features-based feature mapping. Conditional distribution alignment also plays an important role in extracting favorite features for heterogeneous data matching. However, considering the specific characteristics of HDA, such as multi-modalities and different dimensions, DCAN as is cannot directly tackle the difficulties. By designing additional networks or using special kernel functions, DCAN may be extended to adapt HDA tasks.

B. Partial Unsupervised Domain Adaptation

Partial domain adaptation problem is originally proposed by [26], [27], where the target domain label space is a subset of the source domain label space. Recently, several methods

are proposed to deal with partial domain adaptation problem. Importance Weighted Adversarial Net (IWAN) [35] introduces an additional domain classifier to calculate the weight of each sample in the source domain, and then uses GAN to align target domain features with this weighted source domain features. Partial Adversarial Domain Adaptation (PADA) [27] uses the predicted distribution on the target domain to weight the class space of the source domain and then aligns feature space via GAN in the shared label space. Hard Adaptive Feature Norm (HAFN) [24] requires that the feature norms of the source and target domains be close to an identical larger value to complete domain adaptation, thus the assumption of identical label space can be ignored.

C. Conditional Maximum Mean Discrepancy

CMMD is first proposed to deal with supervised learning problems [29]. In this subsection, we briefly review the basic principles of CMMD. Let ϕ and ψ denote the nonlinear mappings for Y and Z , respectively. For the conditional distribution $P(Z|Y)$, given a sample \mathbf{y} , the conditional kernel mean embedding $\mu_{Z|\mathbf{y}}$ can be defined as [36],

$$\mu_{Z|\mathbf{y}} = \mathbb{E}_{Z|\mathbf{y}}[\psi(Z)] = \int_{\Omega} \psi(z)dP(Z|\mathbf{y}) = C_{Z|Y}\phi(\mathbf{y}), \quad (1)$$

where $C_{Z|Y}$ denotes the conditional embedding of $P(Z|Y)$, which can be calculated as,

$$C_{Z|Y} = C_{YZ}C_{Y}^{-1}. \quad (2)$$

C_{YZ} denotes a cross-covariance operator [37], i.e.,

$$C_{YZ} = \mathbb{E}_{YZ}[\phi(Y) \otimes \psi(Z)] - \mu_Y \otimes \mu_Z,$$

where \otimes is the tensor product operator. Given a dataset $\mathcal{D}_{YZ} = (\mathbf{y}_i, \mathbf{z}_i)_{i=1}^n$ from $P(Z|Y)$, $C_{Z|Y}$ can be estimated by $\hat{C}_{Z|Y} = \Psi(\mathcal{K} + \lambda\mathbf{I})^{-1}\Phi^T$, where $\Psi = [\psi(\mathbf{z}_1), \dots, \psi(\mathbf{z}_n)]$, $\Phi = [\phi(\mathbf{y}_1), \dots, \phi(\mathbf{y}_n)]$, $\mathcal{K} = \Phi^T\Phi$ is the kernel function, and λ is a positive regularization parameter.

Based on Eqs. (1) and (2), the conditional distributions are projected to a series of points in the RKHS. Since $\phi(\mathbf{y})$ is a constant vector for a fixed \mathbf{y} , the distance between the conditional kernel mean embeddings can be calculated by comparing the difference between the conditional embeddings. As a result, the CMMD between two conditional distribution $P(Z_1|Y)$ and $P(Z_2|Y)$ is defined as $\|C_{Z_1|Y} - C_{Z_2|Y}\|_{\mathcal{F} \otimes \mathcal{G}}^2$.

III. METHOD

We first introduce the motivation and notations in Section III-A. Then, two important modules in DCAN, i.e., the conditional distribution matching module and the discriminant information extraction module, are introduced in Sections III-B and III-C, respectively. The final objective function and optimization algorithm of DCAN in Section III-D. In addition, Section III-E extends DCAN to address the Partial UDA problem.

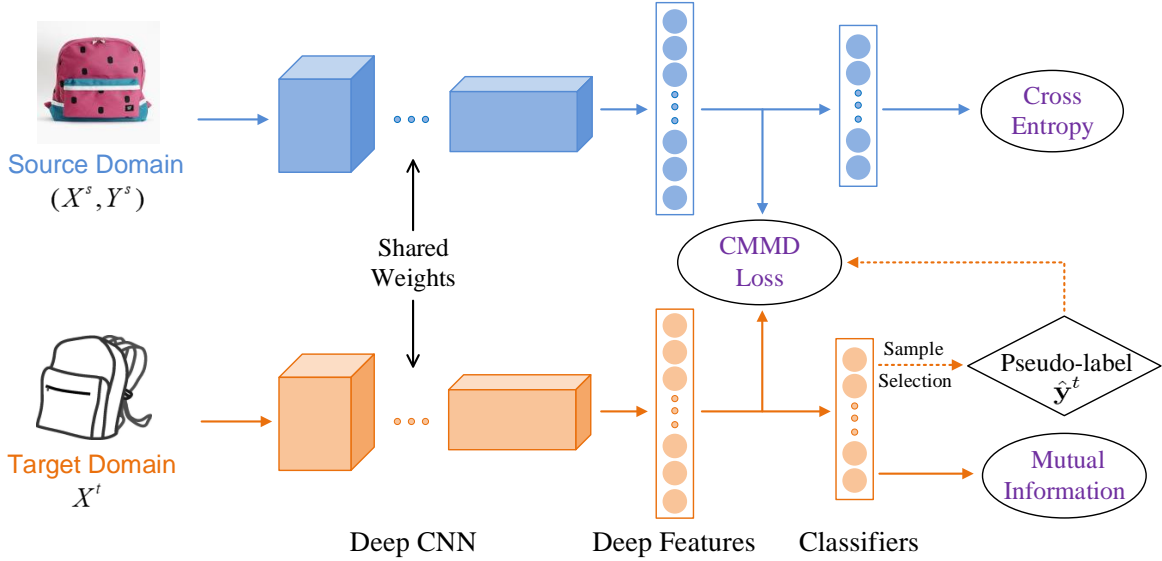


Fig. 2. An overview of DCAN. The source and target domains share network weights of the Deep CNN and Classifier. We obtain the deep features by the Deep CNN, and then input these deep features into the Classifier to get predicted probabilities, which are used to calculate the cross-entropy loss and mutual information. At the same time, we select high-confidential samples in the target domain to assign pseudo-labels. The deep features with the labels and pseudo-labels are then used to estimate the CMMD loss to achieve conditional distributions alignment.

A. Motivation and Notations

The deep feature-level UDA methods assumes that there exists a deep feature space shared by the source domain and the target domain. In this feature space, both the labeled source samples and the unlabeled target samples can be classified as correctly as possible. Generally, this shared feature space should satisfy to the following two characteristics: 1) The feature space should be domain-invariant for each category, which also means conditional distribution alignment. If the source and target domains have the same conditional distribution, then the classifier trained on the source domain can correctly classify samples in the target domain. 2) The feature space should be able to extract discrimination information of the source domain and target domain simultaneously. This would be helpful to alleviate over-fitting on the source domain, thus learning a more generalized predictive model.

In order to learn a feature space which has the two properties as shown above, DCAN contains two interdependent modules: conditional distribution matching and discriminant information extraction. On the one hand, CMMD is used to measure the distance between conditional distributions of the source and target domains, and then the conditional distributions are aligned by minimizing CMMD. On the other hand, in addition to extracting discrimination information of the source domain using the cross-entropy loss, more representative features are captured from the target domain by maximizing the mutual information between samples and the prediction labels.

Several important notations are listed here. In the UDA task, there are generally two related but different datasets, i.e., the source domain $\mathcal{D}_s = (\mathbf{x}_i^s, \mathbf{y}_i^s)_{i=1}^{n_s}$ with n_s labeled samples and the target domain $\mathcal{D}_t = (\mathbf{x}_i^t)_{i=1}^{n_t}$ with n_t unlabeled samples, where \mathbf{y}_i denotes a one-hot encoding vector of the category. Let $P^s(X, Y)$ and $P^t(X, Y)$ represent the joint distribution on the source domain and target domain, respectively. Let

$\mathcal{C}_s = \{1, \dots, c_s\}$ and $\mathcal{C}_t = \{1, \dots, c_t\}$ denote the label space of \mathcal{D}_s and \mathcal{D}_t , respectively. In this paper, we consider a more common UDA scenario where \mathcal{D}_s and \mathcal{D}_t have the same label space but different label distributions, i.e., $\mathcal{C}_s = \mathcal{C}_t$ and $P^s(Y) \neq P^t(Y)$. Furthermore, we also consider the Partial UDA task, which requires $\mathcal{C}_t \subset \mathcal{C}_s$.

B. Conditional Distribution Alignment by CMMD

In this section, we design the conditional distribution matching module with CMMD. The CMMD metric can project the conditional distribution into the Reproducing Kernel Hilbert Space (RKHS), and measure the distance between $P^s(Z|Y)$ and $P^t(Z|Y)$ by calculating the distance between their projections.

Let ϕ and ψ denote the nonlinear mappings for Y and Z , respectively. Then, the kernel mean embedding of $P(Y)$ and $P(Z)$ can be denoted by $\mu_Y = \mathbb{E}_Y[\phi(Y)] = \int_{\Omega} \phi(Y) dP(Y)$ and $\mu_Z = \mathbb{E}_Z[\psi(Z)]$, respectively. We can project a marginal distribution to a point in the RKHS via kernel mean embedding. Similarly, we can project the conditional distribution to a series of points in the RKHS via the conditional kernel mean embedding. Based on Eqs. (1), given a sample \mathbf{y} , the conditional kernel mean embedding of conditional distributions $P^s(Z|Y)$ and $P^t(Z|Y)$ can be defined as,

$$\begin{aligned} \mu_{Z|\mathbf{y}}^s &= \mathbb{E}_{Z^s|\mathbf{y}}[\psi(Z)] = \int_{\Omega} \psi(z) dP^s(Z|\mathbf{y}) = C_{Z|\mathbf{y}}^s \phi(\mathbf{y}), \\ \mu_{Z|\mathbf{y}}^t &= \mathbb{E}_{Z^t|\mathbf{y}}[\psi(Z)] = \int_{\Omega} \psi(z) dP^t(Z|\mathbf{y}) = C_{Z|\mathbf{y}}^t \phi(\mathbf{y}), \end{aligned} \quad (3)$$

where $C_{Z|\mathbf{y}}^s$ and $C_{Z|\mathbf{y}}^t$ denote the conditional embedding of $P^s(Z|Y)$ and $P^t(Z|Y)$, respectively.

To calculate the distance between $P^s(Z|Y)$ and $P^t(Z|Y)$ on the RKHS, we can calculate the distance between $\mu_{Z|\mathbf{y}}^s$ and $\mu_{Z|\mathbf{y}}^t$ by fixing $Y = \mathbf{y}$. Based on the theory of CMMD,

this distance can be calculated by comparing the difference between $C_{Z|Y}^s$ and $C_{Z|Y}^t$. Therefore, the CMMD loss between $P^s(Z|Y)$ and $P^t(Z|Y)$ as be written as,

$$L_{\text{CMMD}} = \|C_{Z|Y}^s - C_{Z|Y}^t\|_{\mathcal{F} \otimes \mathcal{G}}^2. \quad (4)$$

By minimizing the CMMD loss, the difference between conditional distributions of \mathcal{D}_s and \mathcal{D}_t will be reduced. In particular, based on Theorem 3 of [29], when L_{CMMD} reaches its minimum value, $P^s(Z|Y) = P^t(Z|Y)$ for each fixed \mathbf{y} .

In practice, we need to estimate the CMMD loss in a batch-wise manner. To obtain the consistent estimator, we randomly sample two datasets $\mathcal{D}_{YZ}^s = (\mathbf{y}_i^s, \mathbf{z}_i^s)_{i=1}^n$ and $\mathcal{D}_{YZ}^t = (\mathbf{y}_i^t, \mathbf{z}_i^t)_{i=1}^n$ from $P^s(Z|Y)$ and $P^t(Z|Y)$, respectively. Then, an empirical estimation of CMMD between the conditional distribution of the source and target domains can be written as

$$\begin{aligned} \hat{L}_{\text{CMMD}} &= \|\hat{C}_{Z|Y}^s - \hat{C}_{Z|Y}^t\|_{\mathcal{F} \otimes \mathcal{G}}^2 \\ &= \|\Psi_s(\mathcal{K}_s + \lambda \mathbf{I})^{-1} \Phi_s^\top - \Psi_t(\mathcal{K}_t + \lambda \mathbf{I})^{-1} \Phi_t^\top\|_{\mathcal{F} \otimes \mathcal{G}}^2 \\ &= \text{Tr}(\mathcal{K}_s \tilde{\mathcal{K}}_s^{-1} \mathcal{L}_s \tilde{\mathcal{K}}_s^{-1}) + \text{Tr}(\mathcal{K}_t \tilde{\mathcal{K}}_t^{-1} \mathcal{L}_t \tilde{\mathcal{K}}_t^{-1}) \\ &\quad - 2 \cdot \text{Tr}(\mathcal{K}_{ts} \tilde{\mathcal{K}}_s^{-1} \mathcal{L}_{st} \tilde{\mathcal{K}}_t^{-1}), \end{aligned} \quad (5)$$

where $\Psi_s = [\psi(\mathbf{z}_1^s), \dots, \psi(\mathbf{z}_n^s)]$, $\Phi_s = [\phi(\mathbf{y}_1^s), \dots, \phi(\mathbf{y}_n^s)]$, $\mathcal{K}_s = \Phi_s^\top \Phi_s$, $\tilde{\mathcal{K}}_s = \mathcal{K}_s + \lambda \mathbf{I}$, $\mathcal{L}_s = \Psi_s^\top \Psi_s$. Accordingly, Ψ_t , Φ_t , \mathcal{K}_t , $\tilde{\mathcal{K}}_t$ and \mathcal{L}_t are defined on dataset \mathcal{D}_{XY}^t in a similar way. $\mathcal{K}_{ts} = \Phi_t^\top \Phi_s$, $\mathcal{L}_{st} = \Psi_s^\top \Psi_t$.

Notice that the label information in the target domain is required for estimating the L_{CMMD} , which cannot be satisfied in the UDA tasks. As with some UDA methods [38], [39], we obtain pseudo-labels of samples with high confidence in the target domain. In order to improve the representation capacity of the model and the accuracy of pseudo-labels, we use a deep CNN network as feature extractor and a fully-connected network with softmax activation as classifier. Figure 2 shows the network structure of DCAN. During the training process, we first input the samples of the source and target domains into the deep CNN to obtain the deep features, which are then input into the classifier to obtain the predicted labels. The predicted distribution $\hat{\mathbf{y}}_i^t$ for any sample \mathbf{x}_i^t in the target domain is input into a sample selection program. If the maximum value of $\hat{\mathbf{y}}_i^t$ is larger than a threshold γ_0 , we consider this sample as high confidence and then assign this sample corresponding pseudo-label. Finally, the features and pseudo-labels of the selected target domain samples and the features and labels of the source domain samples are combined to calculate the CMMD loss.

C. Discriminant Information Extraction

In Section III-B, we proposed the CMMD-based conditional distribution matching module, which helps to achieve conditional distribution alignment in the shared feature space. On this basis, we expect to learn a more effective model by simultaneously extracting discriminant information in the source and target domains.

As shown in Figure 2, we connect a shared classifier behind the deep CNN to predict the class distribution. Let $P(\hat{Y}|X)$ denote the predicted class distribution. We use cross entropy loss as the classification loss function of the source domain.

Suppose there is a dataset with batch-size n , i.e., $\mathcal{D}_{batch}^s = \{(\mathbf{x}_i^s, \mathbf{y}_i^s)\}_{i=1}^n$, sampled from the source domain \mathcal{D}_s . The cross-entropy loss L_{SC} can be estimated as

$$\hat{L}_{SC} = \frac{1}{n} \sum_{i=1}^n [-P(\mathbf{y}_i^s | \mathbf{x}_i^s) \log P(\hat{\mathbf{y}}_i^s | \mathbf{x}_i^s)]. \quad (6)$$

Now we focus on extracting discriminant information from the target domain, in which all the samples are unlabeled, thus it is difficult to extract classification information by a supervised method. In probability theory and information theory, the mutual information between two variables X and Y measures how much information Y is contained in X . Therefore, we can extract more representative features in the target domain by maximizing the mutual information between X_t and \hat{Y}_t . The mutual information loss L_{MI} of the target domain can be defined as follow,

$$L_{MI} = I(X_t, \hat{Y}_t) = H(\hat{Y}_t) - H(\hat{Y}_t | X_t), \quad (7)$$

in which $H(\hat{Y}_t)$ denotes the information entropy of $P^t(\hat{Y})$ and $H(\hat{Y}_t | X_t)$ denotes the conditional entropy of $P^t(\hat{Y} | X)$. By maximizing the mutual information loss, we simultaneously minimize the entropy of category conditional distribution and maximize the entropy of category marginal distribution. In the UDA literature [15], [24], the entropy of conditional distribution, also known as low-density separation criterion, has been used to constrain the classification boundary trained on the source domain through the low density region of the target domain feature space to prevent over-fitting. However, minimizing the entropy of the conditional distribution may result in excessive aggregation of the samples, further result in multiple categories of samples being grouped into one category. Different from these methods, we also maximize the entropy of marginal distribution to alleviate class imbalance problem and extract more discrimination features.

In practice, given a dataset with batch-size n , i.e., $\mathcal{D}_{batch}^t = \{(\mathbf{x}_i^t)\}_{i=1}^n$, sampled from the target domain \mathcal{D}_t , we can obtain the corresponding prediction classification probability $P(\hat{\mathbf{y}}_i^t | \mathbf{x}_i^t)$ through the deep network. Then, the mutual information loss can be estimated as

$$\hat{L}_{MI} = H\left[\frac{1}{n} \sum_{i=1}^n P(\hat{\mathbf{y}}_i^t | \mathbf{x}_i^t)\right] - \frac{1}{n} \sum_{i=1}^n H[P(\hat{\mathbf{y}}_i^t | \mathbf{x}_i^t)]. \quad (8)$$

D. DCAN & Training Procedure

Now we can define the objective function of DCAN by combining these three loss functions (4), (6), (7) as follow,

$$\min_{\mathbf{w}} L_{SC} + \lambda_0 L_{\text{CMMD}} - \lambda_1 L_{MI}, \quad (9)$$

where \mathbf{w} denotes all the network parameters in the deep network, λ_0 and λ_1 are hyper-parameters.

DCAN consists of two successive training phases. First, to ensure that the deep network can obtain more high-confidence pseudo-labels at the initial transfer, we pre-train the deep network using the samples in the source domain. Next, we minimize the objective function (9) by mini-batch stochastic

gradient descent method. Based on the chain rule, the gradient of the loss function on a mini-batch can be written as

$$\sum_{i=1}^n \left[\left(\frac{\partial \hat{\mathbf{y}}_i^s}{\partial \mathbf{w}} \right)^\top \frac{\partial \hat{L}_{SC}}{\partial \hat{\mathbf{y}}_i^s} - \lambda_1 \left(\frac{\partial \hat{\mathbf{y}}_i^t}{\partial \mathbf{w}} \right)^\top \frac{\partial \hat{L}_{MI}}{\partial \hat{\mathbf{y}}_i^t} + \lambda_0 \sum_{j=1}^n \left(\frac{\partial \hat{L}_{CMMD}}{\partial z_{ij}^s} \frac{\partial z_{ij}^s}{\partial \mathbf{w}} + \frac{\partial \hat{L}_{CMMD}}{\partial z_{ij}^t} \frac{\partial z_{ij}^t}{\partial \mathbf{w}} \right) \right],$$

where z_{ij} denotes the j -th dimensional feature representation of \mathbf{x}_i . For simplicity, the gradients of \hat{L}_{SC} and \hat{L}_{MI} are omitted here. For CMMD, Eq. (5) can be expressed as

$$\hat{L}_{CMMD} = \text{Tr}(G_s \mathcal{L}_s) + \text{Tr}(G_t \mathcal{L}_t) - 2 \cdot \text{Tr}(G_{ts} \mathcal{L}_{st}),$$

where $G_s = \tilde{\mathcal{K}}_s^{-1} \mathcal{K}_s \tilde{\mathcal{K}}_s^{-1}$, $G_t = \tilde{\mathcal{K}}_t^{-1} \mathcal{K}_t \tilde{\mathcal{K}}_t^{-1}$ and $G_{ts} = \tilde{\mathcal{K}}_t^{-1} \mathcal{K}_{ts} \tilde{\mathcal{K}}_s^{-1}$. Since G_s , G_t and G_{ts} are constant matrices, $\frac{\partial \hat{L}_{CMMD}}{\partial z_{ij}^s}$ can be calculated as,

$$\begin{aligned} \frac{\partial \hat{L}_{CMMD}}{\partial z_{ij}^s} &= \frac{\partial \text{Tr}(G_s \mathcal{L}_s)}{\partial z_{ij}^s} - 2 \cdot \frac{\partial \text{Tr}(G_{ts} \mathcal{L}_{st})}{\partial z_{ij}^s} \\ &= \text{Tr}(G_s \frac{\partial \mathcal{L}_s}{\partial z_{ij}^s}) - 2 \cdot \text{Tr}(G_{ts} \frac{\partial \mathcal{L}_{st}}{\partial z_{ij}^s}). \end{aligned}$$

Similarly, $\frac{\partial \hat{L}_{CMMD}}{\partial z_{ij}^t}$ can also be computed. All the gradients can be easily computed in the Pytorch framework. The overall algorithm of DCAN is summarized in Algorithm 1.

Algorithm 1 DCAN for UDA

Input: $\mathcal{D}_s = \{(\mathbf{x}_i^s, \mathbf{y}_i^s)\}_{i=1}^{n_s}$, $\mathcal{D}_t = \{\mathbf{x}_i^t\}_{i=1}^{n_t}$.

Output: The network parameters \mathbf{w} .

- 1: Pre-train the deep network with samples in \mathcal{D}_s .
 - 2: **while** not converged **do**
 - 3: Random sample a mini-batch \mathcal{D}_{batch}^s and \mathcal{D}_{batch}^t from \mathcal{D}_s and \mathcal{D}_t , respectively;
 - 4: Generate $\hat{\mathbf{y}}_i^t$ for each sample $\mathbf{x}_i^t \in \mathcal{D}_{batch}^t$ by current classifier, and predict pseudo-labels for samples with high confidence;
 - 5: Estimate the CMMD loss, cross-entropy loss and mutual information loss by Eqs. (5), (6), and (8), respectively;
 - 6: Compute the gradients of Eqs. (5), (6), and (8) w.r.t. \mathbf{w} on \mathcal{D}_{batch}^s and \mathcal{D}_{batch}^t ;
 - 7: Update \mathbf{w} by gradient descend to minimize Eq. (9);
 - 8: **end while**
-

E. Extension to Deal with the Partial UDA Problem

In this subsection, we extend the DCAN algorithm to accommodate the Partial UDA tasks. As shown above, the objective of CDAN contains three loss functions, i.e., CMMD loss for conditional distribution alignment, cross-entropy loss for extracting discriminant information of \mathcal{D}_s , and mutual information loss for extracting more representative information of \mathcal{D}_t . The CMMD loss and cross-entropy loss are unaffected by the change of the label space and thus can be used in the Partial UDA task. The mutual information loss can be decomposed into the difference between $H(\hat{Y}_t)$ and $H(\hat{Y}_t|X_t)$. In the partial setting, we cannot accurately estimate $P(Y_t)$ by

$P(\hat{Y}_t)$, Thus the mutual information loss needs to be modified to accommodate the Partial UDA task.

In the partial setting, maximizing $H(P(\hat{Y}_t))$ will cause the target domain samples to be distributed evenly to each category of \mathcal{D}_s , which perhaps result in negative transfer. To solve this problem, one method is to remove the constraint on $H(P(\hat{Y}_t))$. However, as we mentioned above, minimizing $H(P(\hat{Y}_t|X_t))$ may lead to excessive aggregation of samples in \mathcal{D}_t , and maximizing $H(P(\hat{Y}_t))$ can help to mitigate this problem. To avoid the excessive aggregation of target domain samples, we introduce a threshold γ_1 to control the effect of $H(P(\hat{Y}_t))$. When $H(P(\hat{Y}_t)) < \gamma_1$, we maximize $H(P(\hat{Y}_t))$ to ensure class balance, and when $H(P(\hat{Y}_t)) > \gamma_1$, we remove the effect of $H(P(\hat{Y}_t))$. The mutual information loss under the partial setting is

$$L_{MI}^P = \min\{H(\hat{Y}_t), \gamma_1\} - H(\hat{Y}_t|X_t). \quad (10)$$

The objective function of Partial DCAN is then formulated by

$$\min_{\mathbf{w}} L_{SC} + \lambda_0 L_{CMMD} - \lambda_1 L_{MI}^P. \quad (11)$$

Eq. (11) can be optimized in an end-to-end manner, and the main steps for addressing Partial UDA are shown in Algorithm 2.

Algorithm 2 DCAN for Partial UDA

Input: $\mathcal{D}_s = \{(\mathbf{x}_i^s, \mathbf{y}_i^s)\}_{i=1}^{n_s}$, $\mathcal{D}_t = \{\mathbf{x}_i^t\}_{i=1}^{n_t}$.

Output: The network parameters \mathbf{w} .

- 1: Pre-train the deep network with samples in \mathcal{D}_s .
 - 2: **while** not converged **do**
 - 3: Random sample a mini-batch \mathcal{D}_{batch}^s and \mathcal{D}_{batch}^t from \mathcal{D}_s and \mathcal{D}_t , respectively;
 - 4: Generate $\hat{\mathbf{y}}_i^t$ for each sample $\mathbf{x}_i^t \in \mathcal{D}_{batch}^t$ by current classifier, and predict pseudo-labels for samples with high confidence;
 - 5: Estimate the CMMD loss, cross-entropy loss and partial mutual information loss by Eqs. (5), (6), and (10), respectively;
 - 6: Compute the gradients of Eqs. (5), (6), and (10) w.r.t. \mathbf{w} on \mathcal{D}_{batch}^s and \mathcal{D}_{batch}^t ;
 - 7: Update \mathbf{w} by gradient to minimize Eq. (11);
 - 8: **end while**
-

IV. EXPERIMENT RESULTS AND ANALYSIS

In this section, we evaluate DCAN method on four visual datasets. We first test its classification accuracy on UDA and Partial UDA tasks, and compare it with several state-of-the-art deep learning methods. Then, we evaluate its effectiveness from several views, i.e., parameter sensitivity, evaluation of each component, impact of the number of classes, feature visualization and time complexity.

A. Datasets and Experimental Setup

All experiments are conducted on four visual datasets, i.e., Digit, Office-31, ImageCLEF-DA and Office-Home, which are widely used to test DA algorithms. Some image samples of these datasets are shown in Figure 3.



Fig. 3. Sample images of four datasets, Digit Datasets, Office-31, ImageCLEF-DA and Office-Home. Samples in the same row belong to the same domain, and samples in the same column belong to the same class.

Digit Datasets contains 10 categories of digital images (0-9) from three domains, i.e., MNIST [40], USPS [41] and SVHN [42]. MNIST includes 70,000 handwritten digital images of 10 classes, and each image has 28×28 size. USPS is also handwritten digital images dataset, which consists of 9,298 gray images with size of 16×16 . SVHN consists of 73257 color digital images with size of $3 \times 32 \times 32$, which are all captured from house numbers. We conduct three widely-used UDA tasks (i.e., MNIST \rightarrow USPS, USPS \rightarrow MNIST and SVHN \rightarrow MNIST) to evaluate the DCAN method. Specifically, we follow the protocol established in literature [12], and randomly sample 2000 samples from MNIST and 1800 samples from USPS in the UDA experiments between MNIST and USPS.

ImageCLEF-DA¹ dataset includes 1791 real scenes images in 12 common categories which are shared by the following three domains, i.e., ImageNet (I), Pascal VOC (P), and Caltech-256 (C). On this dataset, we evaluate DCAN method across all six UDA tasks.

Office-31 [43] is the most popular dataset for UDA task, which collects 4,110 images of office supplies in 31 classes from three distinct domains: Amazon (A) consisting of online web images, DSLR (D) consisting of digital SLR camera images, and Webcam (W) consisting of web camera images. In order to conduct the Partial UDA experiment, we follow the literature [27] to use the common sub-dataset from Office-31 and Office-10 as target domain. We evaluate DCAN method across all six UDA tasks and six Partial UDA tasks.

Office-Home [44] is a more challenging dataset for UDA task, which contains 15588 images of common objects in 65 categories from four different areas: Art (Ar), Clipart (Cl), Product (Pr) and Real-World (Rw). In the Partial UDA task, we follow the setting in literature [27] to use all the samples of a domain as the source domain, and the samples from the first 25 categories (in alphabetic order) in another domain as the target domain. We conduct all 12 UDA tasks and 12 Partial UDA tasks to evaluate DCAN method.

In the MNIST \rightarrow USPS and USPS \rightarrow MNIST tasks, we resize the samples in USPS to 28×28 to match the MNIST image size. For the SVHN \rightarrow MNIST task, we resize the MNIST images to 32×32 and then extend these images to three channels to match the image size in SVHN. In the rest of the

tasks, we use a unified data processing protocol. Specifically, for an image, we use the following four operations in turn: 1) resize this image to $3 \times 224 \times 224$, 2) horizontally flip this image randomly with a probability of 0.5, 3) convert this image in the range $[0, 255]$ to a tensor in the range $[0.0, 1.0]$, 4) normalize this tensor with mean $[0.485, 0.456, 0.406]$ and standard deviation $[0.229, 0.224, 0.225]$.

Some implementation details are summarized as follows. In the transfer tasks of the digital datasets, we use the simple modified LeNet [40] used in literatures [16], [23] as the baseline network structure and randomly initialize the network weights. In the other transfer tasks, we follow the setting in benchmark approaches [17], [32] and use the Pytorch-provided ResNet-50 [45] pre-trained model as the baseline network structure. In all experiments, we fix the hyper-parameters as $\lambda_0 = 0.1$, $\lambda_1 = 0.2$, $\gamma_0 = 0.95$, $\gamma_1 = 1.5$ and the batch-size as $n = 32$. To estimate the CMMD loss, we use a mixture kernel function obtained from an average of five Gaussian kernels, where the bandwidth is set to 0.1, 1, 10, 100, and 1000, respectively. We replace the fully connected (FC) layer of ResNet-50 with a FC network to accommodate the new category number. Specifically, we use one FC-layer for Office-Home, while two FC-layers (2048-512-31) for Office-31 and ImageCLEF-DA. For digital transfer tasks, we use ADAM optimization algorithm [46] with learning rate $2e-4$. For the other three datasets, we set a learning rate of $2e-4$ for the FC-layers, while the other layers are $2e-5$. We follow the standard training and evaluation settings in UDA, i.e., using the labeled samples of \mathcal{D}_s and the unlabeled samples of \mathcal{D}_t for training, and then testing the classification accuracy in \mathcal{D}_t . In each experiment, we repeat DCAN three times with different random initialization, and report the mean accuracy and standard deviation following [24].

B. Experiment Results on UDA Tasks

In this section, we report the classification performance of DCAN on the UDA tasks, and compare it with several state-of-the-art methods, e.g., ResNet [45], DAN [15], BDA [31], DDC [14], DANN [16], Deep Reconstruction-Classification Network (DRCN) [47], Coupled Generative Adversarial Network (CoGAN) [18], Generate To Adapt (GTA) [48], RTN [17], ADDA [23], JAN [30], WDAN [25], Conditional Domain Adversarial Networks (CDAN) [32]. For

¹<http://imageclef.org/2014/adaptation>

TABLE I
COMPARISON WITH STATE-OF-THE-ART METHODS ON THE DIGIT
DATASETS FOR UNSUPERVISED DOMAIN ADAPTATION.

Method	SVHN→MNIST	MNIST→USPS	USPS→MNIST
LeNet [40]	60.1±0.01	75.2±0.01	57.1±0.02
BDA [31]	-	88.56	82.8
DANN [16]	73.9	77.1±1.8	73.0±2.0
DRCN [47]	82.0±0.16	91.8±0.09	73.7±0.04
CoGAN [18]	-	91.2±0.8	89.1±0.8
ADDA [23]	76.0±1.8	89.4±0.2	90.1±0.8
WDAN [25]	80.5±2.5	90.2±0.1	89.2±0.5
GTA [48]	92.4±0.9	92.8±0.9	90.8±1.3
DCAN(ours)	98.45±0.1	96.11±0.1	96.87±0.1

a fair comparison, the same network protocol is used to evaluate the performance of BDA [31] and WDAN [25]. For the rest methods, the reported results are cited from the original papers or from [30].

We first evaluate DCAN on three tasks of the digital datasets, i.e., SVHN→MNIST, MNIST→USPS and USPS→MNIST. The results are shown in Table I. We can see that DCAN achieves state-of-the-art results in all three tasks. In particular, the average classification accuracies of DCAN on these tasks are 98.45%, 96.11% and 96.87%, which outperform the second best results by 6.05%, 3.31% and 6.07%.

Tables II and III show the results of DCAN on six tasks of Office-31 dataset and six tasks of ImageCLEF-DA dataset, respectively. We can see that DCAN achieves comparable performance on all of these tasks. DCAN achieves the average classification accuracies over all six tasks of 88.1% and 89.0%, which are 0.4% and 1.3% better than the state-of-the-art method CDAN, respectively. In particular, for the more difficult transfer tasks, such as D→A, W→A in Office-31 and P→I, C→P in ImageCLEF-DA, DCAN improves the average accuracy by about 3%, which further validates the effectiveness of our method.

Office-Home contains 65 different categories, and the category distribution difference across different domains are even larger, thus it provides a more challenging UDA benchmark. Table IV shows classification accuracies of DCAN and the compared methods on all 12 transfer tasks. Note that DCAN reports the average accuracy and standard deviation over three run cycles, while the compared methods report the optimal accuracy. We obtain the following observations from Table IV: 1) Marginal distribution alignment-based methods, such as DAN and DANN, perform poorly in Office-Home, and it can be attributed to the negative migration phenomenon. 2) CADN uses Conditional GAN to align feature spaces and achieves better performance than DANN and ADDA, which verifies the role of conditional distribution matching in UDA tasks. 3) Our DCAN uses CMMD to directly measure the difference between two conditional distributions, which is more effective than BDA, WDAN and CDAN. Experiment results validate the effectiveness of our method. As we can see from Table IV, the average accuracy of DCAN is 71.17%, which is 5.37% higher than the compared approaches.

C. Experiment Results on Partial UDA Tasks

In this section, we report the performance of DCAN on the partial UDA tasks, and compare it with several state-of-the-art methods, i.e. ResNet [45], DAN [15], DANN [16], ADDA [23], RTN [17], JAN [30], BDA [31], IWAN [35], PADA [27], Two Weighted Inconsistency-reduced Networks (TWINs) [49], WDAN [25], HAFN [24] and Instance Adaptive Feature Norm (IAFN) [24]. For a fair comparison, the same network backbone is used to evaluate the performance of BDA [31] and WDAN [25]. For the rest methods, the reported results are cited from the original papers or from [27].

Under the Partial UDA settings, the classification accuracy on 6 tasks of the Office-31 dataset and 12 tasks of the Office-Home dataset are shown in Tables V and VI, respectively. We observe that the classification results obtained by marginal distribution alignment-based methods, such as DANN, ADDA and JAN, are even worse than directly finetune the ResNet-50. It indicates that marginal distribution alignment is seriously affected by negative transfer. Our DCAN uses conditional distributions, rather than marginal distributions, to achieve feature space alignment, thus it avoids the negative transfer effect. For Office-31, Our DCAN surpasses other algorithms on most tasks, and the average of all six tasks achieves 95.04%, which exceeds the second-order method by 1.44%. For Office-Home, DCAN improves significantly compared to the state-of-the-art methods, and increase by 4.51% in the average of all 12 tasks. These indicate that our new method can handle the Partial UDA Problems effectively.

D. Effectiveness Analysis

1) *Parameter Sensitivity*: There are four important hyper-parameters in DCAN, i.e., λ_0 , λ_1 , γ_0 and γ_1 . To evaluate the sensitivity of CDAN against these hyper-parameters, we run CDAN with $\lambda_0 \in \{0.01, 0.05, 0.1, 0.5, 1\}$, $\lambda_1 \in \{0.01, 0.1, 0.2, 0.5, 1\}$, $\gamma_0 \in \{0.3, 0.6, 0.9, 0.95, 0.99\}$, and $\gamma_1 \in \{0.5, 1, 1.5, 2, 2.5\}$. We investigate λ_0 , λ_1 and γ_0 with the UDA tasks on Office-31 and investigate γ_1 with the Partial UDA tasks on Office-Home. The experiment results are shown in Figure 4. From Figures 4(a) and 4(b), we can see that the accuracy of DCAN has a similar trend for a majority of tasks when hyper-parameters λ_0 and λ_1 vary. The best choice of weight hyper-parameters λ_0 , λ_1 are 0.1 and 0.2, respectively. γ_0 is the threshold for controlling pseudo-labels generation. A small threshold will reduce the accuracy of pseudo-labels, while a large threshold will reduce the number of pseudo-labels, thus a suitable threshold can neither be too large nor too small. The results shown in Figure 4(c) validate our motivation that the classification accuracy first increases and then decreases, and DCAN obtains the best results when $\gamma_0 \in \{0.9, 0.95\}$. γ_1 is used to control the entropy of $P(\hat{Y})$ in Partial DCAN. From Figure 4(d), we observe that DCAN obtains a robust result against γ_1 , and the optimal parameter is selected from $\{1, 1.5, 2\}$.

2) *Feature Visualization*: We use the t-SNE [50] method to visualize the embedding subspace of different methods in the R→P task on the Office-Home dataset. The results are

TABLE II
COMPARISON WITH STATE-OF-THE-ART METHODS ON OFFICE-31 FOR UNSUPERVISED DOMAIN ADAPTATION (RESNET-50).

Method	A→W	D→W	W→D	A→D	D→A	W→A	Avg
Resnet-50 [45]	68.4±0.2	96.7±0.1	99.3±0.1	68.9±0.2	62.5±0.3	60.7±0.3	76.1
DAN [15]	80.5±0.4	97.1±0.2	99.6±0.1	78.6±0.2	63.6±0.3	62.8±0.2	80.4
DDC [14]	75.6±0.2	96.0±0.2	98.2±0.1	76.5±0.3	62.2±0.4	61.5±0.5	78.3
BDA [31]	83.4	97.5	99.6	80.5	67.7	68.7	82.9
DANN [16]	82.0±0.4	96.9±0.2	99.1±0.1	79.7±0.4	68.2±0.4	67.4±0.5	82.2
RTN [17]	84.5±0.2	96.8±0.1	99.4±0.1	77.5±0.3	66.2±0.2	64.8±0.3	81.6
ADDA [23]	86.2±0.5	96.2±0.3	98.4±0.3	77.8±0.3	69.5±0.4	68.9±0.5	82.9
JAN [30]	85.4±0.3	97.4±0.2	99.8±0.2	84.7±0.3	68.6±0.3	70.0±0.4	84.3
WDAN [25]	84.3±0.4	98.0±0.3	99.9±0.6	80.4±0.6	66.0±1.8	62.3±1.0	82.0
GTA [48]	89.5±0.5	97.9±0.3	99.8±0.4	87.7±0.5	72.8±0.3	71.4±0.4	86.5
CDAN [32]	93.1±0.2	98.2±0.2	100±0.0	89.8±0.3	70.1±0.4	68.0±0.4	86.6
CDAN+E [32]	94.1±0.1	98.6±0.1	100±0.0	92.9±0.2	71.0±0.3	69.3±0.3	87.7
DCAN(ours)	92.7±0.4	98.4±0.1	100±0.0	90.7±0.3	73.5±0.2	73.4±0.4	88.1

TABLE III
COMPARISON WITH STATE-OF-THE-ART METHODS ON IMAGECLEF-DA FOR UNSUPERVISED DOMAIN ADAPTATION (RESNET-50).

Method	I→P	P→I	I→C	C→I	C→P	P→C	Avg
ResNet-50 [45]	74.8±0.3	83.9±0.1	91.5±0.3	78.0±0.2	65.5±0.3	91.2±0.3	80.7
DAN [15]	74.5±0.4	82.2±0.2	92.8±0.2	86.3±0.4	69.2±0.4	89.8±0.4	82.5
BDA [31]	75.0	79.5	91.5	83.7	71.7	84.5	81.0
DANN [16]	75.0±0.6	86.0±0.3	96.2±0.4	87.0±0.5	74.3±0.5	91.5±0.6	85.0
RTN [17]	74.6±0.3	85.8±0.1	94.3±0.1	89.5±0.3	71.7±0.3	91.2±0.4	83.9
JAN [30]	76.8±0.4	88.0±0.2	94.7±0.2	89.5±0.3	74.2±0.3	91.7±0.3	85.8
WDAN [25]	77.1±0.7	91.3±0.3	94.4±0.4	89.3±0.3	73.2±0.2	94.5±0.4	86.6
CDAN [32]	76.7±0.3	90.6±0.3	97.0±0.4	90.5±0.4	74.5±0.3	93.5±0.4	87.1
CDAN+E [32]	77.7±0.3	90.7±0.2	97.7±0.3	91.3±0.3	74.2±0.2	94.3±0.3	87.7
DCAN(ours)	77.8±0.5	93.3±0.4	96.9±0.1	91.9±0.1	77.9±0.3	96.2±0.2	89.0

TABLE IV
COMPARISON WITH STATE-OF-THE-ART METHODS ON OFFICE-HOME FOR UNSUPERVISED DOMAIN ADAPTATION (RESNET-50).

Method	A→C	A→P	A→R	C→A	C→P	C→R	P→A	P→C	P→R	R→A	R→C	R→P	Avg
Resnet-50 [45]	34.9	50.0	58.0	37.4	41.9	46.2	38.5	31.2	60.4	53.9	41.2	59.9	46.1
DAN [15]	43.9	57.0	67.9	45.8	56.5	60.4	44.0	43.6	67.7	63.1	51.5	74.3	56.3
BDA [31]	46.4	64.8	67.8	42.1	60.9	61.7	49.7	43.3	71.2	59.0	50.5	77.1	57.9
DANN [16]	45.6	59.3	70.1	47.0	58.5	60.9	46.1	43.7	68.5	63.2	51.8	76.8	57.6
JAN [30]	45.9	61.2	68.9	50.4	59.7	61.0	45.8	43.4	70.3	63.9	52.4	76.8	58.3
WDAN [25]	47.1	69.1	74.0	58.0	64.9	68.8	53.7	45.6	75.6	67.4	53.3	80.4	63.2
CDAN [32]	49.0	69.3	74.5	54.4	66.0	68.4	55.6	48.3	75.9	68.4	55.4	80.5	63.8
CDAN+E [32]	50.7	70.6	76.0	57.6	70.0	70.0	57.4	50.9	77.3	70.9	56.7	81.6	65.8
DCAN(ours)	57.95	76.17	79.28	67.27	76.08	75.61	65.37	55.99	80.67	74.18	61.18	84.23	71.17
	±0.33	±0.03	±0.17	±0.16	±0.26	±0.15	±0.08	±0.22	±0.10	±0.27	±0.60	±0.34	

shown in Figure 5. As shown in Figure 5(a), the Source-Only model cannot align feature spaces effectively because of the domain discrepancy. Figures 5(b) and 5(c) show the embedding space of DCAN and Partial DCAN, respectively. We obtain the following observations: 1) DCAN achieves conditional distribution alignment very well. 2) The inter-class scatter in the feature space of DCAN is larger. It indicates that DCAN can simultaneously achieve conditional distribution alignment and discriminant information extraction.

3) *Evaluation of Each Component*: In order to achieve conditional distribution matching, DCAN contains three loss functions: 1) cross-entropy loss to extract discriminant information in the source domain, 2) CMMD loss to minimize the difference between conditional distributions, and 3) mutual information loss to extract target discrimination information from the target domain. Compared with other UDA methods, DCAN mainly introduces two new terms, i.e., CMMD and $H(P(\hat{Y}))$. Let No-CMMD and No-H2 denote the DCAN models without CMMD and $H(P(\hat{Y}))$, respectively. We eval-

uate the performance of these models on the UDA tasks and the Partial UDA tasks. Experiment results are shown in Figure 6. We observe that the performance of No-CMMD and No-H2 is better than Source-Only, but worse than DCAN. This indicates the importance of CMMD and $H(P(\hat{Y}))$ for improving classification performance in both UDA and Partial UDA tasks. In Figure 6(b), we observe that the performance of No-CMMD is worse than No-H2 under the Partial UDA setting. This indicates that CMMD is more important than $H(P(\hat{Y}))$ when the label distribution difference between source and target domains is large.

4) *Effects of Batch-size*: During the training process of DCAN, we need to estimate CMMD and mutual information on a mini-batch dataset. The accuracy of these estimators depends on the batch-size n . To test the effects of the setting of batch-size, we run DCAN with different batch-sizes $n \in \{8, 16, 32, 64, 128\}$. The experiment results are shown in Figure 7. It can be observed that DCAN achieves a robust classification performance with regard to a wide range of

TABLE V
COMPARISON WITH STATE-OF-THE-ART METHODS ON OFFICE-31 FOR PARTIAL UNSUPERVISED DOMAIN ADAPTATION (RESNET-50).

Method	A→W	D→W	W→D	A→D	D→A	W→A	Avg
Resnet-50 [45]	54.5	94.6	94.3	65.6	73.2	71.7	75.6
DAN [15]	46.4	53.6	58.6	42.7	65.7	65.3	55.4
DANN [16]	41.4	46.8	38.9	41.4	41.3	44.7	42.4
ADDA [23]	43.7	46.5	40.1	43.7	42.8	46.0	43.8
RTN [17]	75.3	97.1	98.3	66.9	85.6	85.7	84.8
JAN [30]	43.4	53.6	41.4	35.7	51.0	51.6	46.1
BDA [31]	77.6	95.6	98.7	82.2	86.5	86.4	87.8
PADA [27]	86.5	99.3	100	82.2	92.7	95.4	92.7
WDAN [25]	85.1	98.9	100	84.7	94.0	92.8	92.6
TWINs [49]	86.0	99.3	100	86.8	94.7	94.5	93.6
DCAN(ours)	90.51 ±1.03	99.78 ±0.19	100 ±0.00	88.73 ±0.38	95.09 ±0.31	95.03±0.24	95.04

TABLE VI
COMPARISON WITH STATE-OF-THE-ART METHODS ON OFFICE-HOME FOR PARTIAL UNSUPERVISED DOMAIN ADAPTATION (RESNET-50).

Method	A→C	A→P	A→R	C→A	C→P	C→R	P→A	P→C	P→R	R→A	R→C	R→P	Avg
Resnet-50 [45]	38.57	60.78	75.21	39.94	48.12	52.90	49.68	30.91	70.79	65.38	41.79	70.42	53.71
DAN [15]	44.36	61.79	74.49	41.78	45.21	54.11	46.92	38.14	68.42	64.37	45.37	68.85	54.48
DANN [16]	44.89	54.06	68.97	36.27	34.34	45.22	44.08	38.03	68.69	52.98	34.68	46.50	47.39
RTN [17]	49.37	64.33	76.19	47.56	51.74	57.67	50.38	41.45	75.53	70.17	51.82	74.78	59.25
BDA [31]	46.17	63.53	73.00	55.65	55.69	63.22	52.43	41.73	71.45	59.23	50.21	73.73	58.84
PADA [27]	51.95	67.00	78.74	52.16	53.78	59.03	52.61	43.22	78.79	73.73	56.60	77.09	62.06
WDAN [25]	52.42	74.51	81.28	63.73	66.11	72.39	63.08	51.34	80.34	73.00	56.24	80.00	67.87
HAFN [24]	53.35	72.66	80.84	64.16	65.34	71.07	66.08	51.64	78.26	73.45	55.28	79.02	67.51
	±0.44	±0.53	±0.50	±0.48	±0.30	±1.04	±0.68	±0.42	±0.51	±0.13	±0.37	±0.19	
IAFN [24]	58.93	76.25	81.42	70.43	72.97	77.78	72.36	55.34	80.40	75.81	60.42	79.92	71.83
	±0.50	±0.33	±0.27	±0.46	±1.39	±0.52	±0.31	±0.46	±0.78	±0.37	±0.83	±0.20	
DCAN(ours)	60.18	85.30	89.01	73.77	76.88	83.64	71.66	59.40	88.04	79.55	63.28	85.34	76.34
	±0.12	±0.21	±0.06	±0.39	±1.00	±0.14	±0.19	±0.59	±0.42	±0.19	±0.84	±0.44	

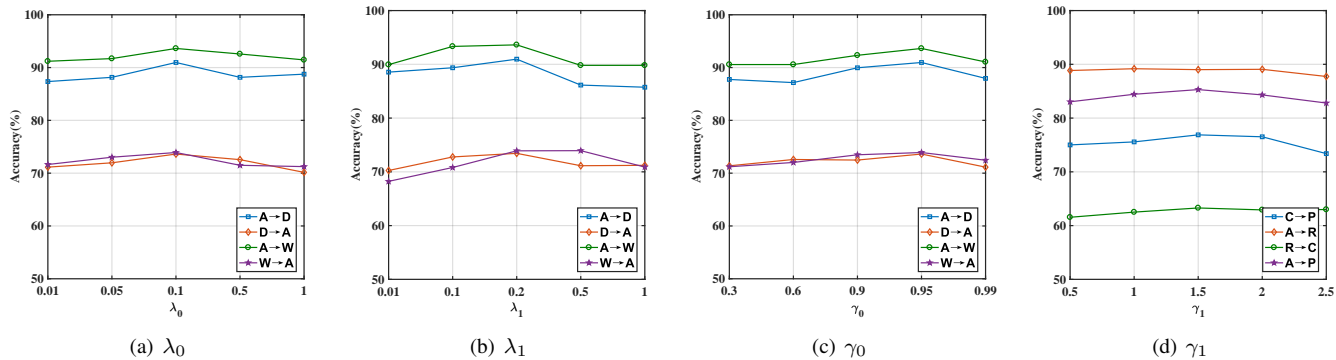


Fig. 4. (a)~(c) Sensitivity of DACN on UDA tasks to the hyper-parameter $\lambda_0, \lambda_1, \gamma_0$, respectively. (d) Sensitivity of DACN on Partial UDA tasks to the hyper-parameter γ_1 .

n values, and the classification performance of DCAN is degenerated when the value of batch-size is particularly small, such as $n = 8$. This demonstrates the robustness of DCAN under the batch-size n . It also indicates that we do not need to deliberately fine-tune the batch-size in real implementations.

5) *DCAN with Ground Truth Labels*: When estimating the CMMD between the conditional distributions, we replace the missing label information on the target domain with pseudo-labels, which affects the accuracy of the CMMD estimator. To further verify the effectiveness of DCAN, we evaluate the classification performance of DCAN on Office-31 when the ground truth labels of target domain are used to estimate CMMD during training. The results are shown in Figure 8. The classification performance of DCAN with real labels is greatly improved compared to DCAN with pseudo-labels. On

A→W and A→D tasks, the classification accuracy of DCAN with real labels is close to 100%. On more challenging W→A and D→A tasks, the classification accuracy of DCAN with real labels increases by about 20%. These results indicate that DCAN can effectively transfer the classification information by aligning conditional distributions when the ground truth of target labels are given.

6) *Number of Classes in Target Domain*: We evaluate the impact of category number in the target domain. Figure 9 shows the experiment results of three methods, i.e., Source-Only, DANN [16] and DCAN, in the C→P task of Office-Home dataset. In this experiment, the source domain has 65 different categories, and the category number in the target domain is gradually reduced from 65 to 5. We see that as the category number decreases, the classification accuracy of

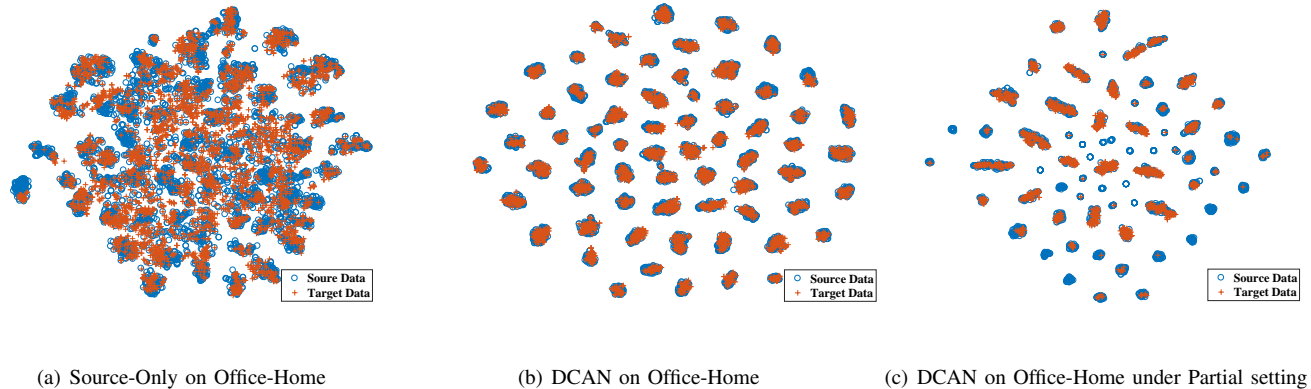


Fig. 5. T-SNE visualization in the task $R \rightarrow P$ on Office-Home dataset. (a) Visualization of Source-Only model. (b) T-SNE visualization of our DCAN. (c) T-SNE visualization of our DCAN under partial setting. The circle and plus represent the source and target samples, respectively. Better viewed in color.

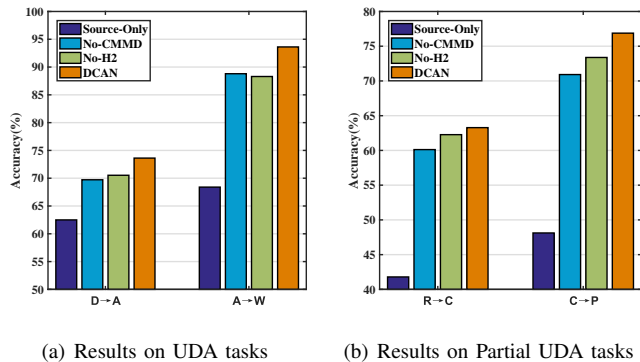


Fig. 6. (a) Evaluation of each component on UDA tasks. (b) Evaluation of each component on Partial UDA tasks.

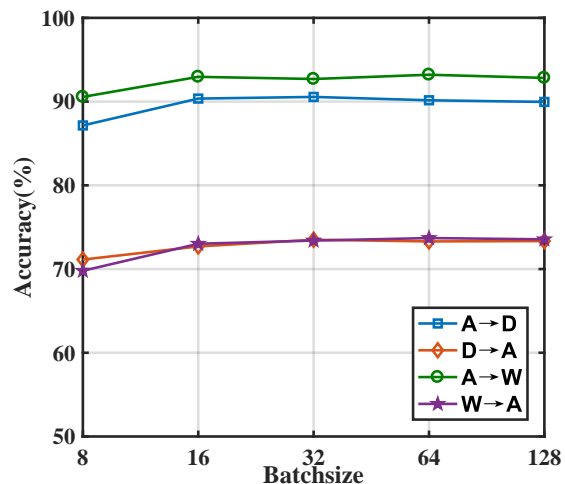


Fig. 7. Sensitivity of DACN to the batch-size n on Office-31.

DANN gradually decreases, even lower than the Source-Only model. Our DCAN shows robustness against the category number in the target domain, and achieves more than 75% classification accuracy on all tasks. This indicates the effective-

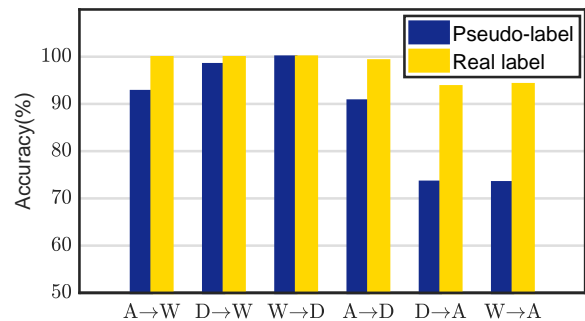


Fig. 8. The classification performance of DCAN on Office-31 dataset when pseudo-labels and real labels are used to estimate CMMD, respectively.

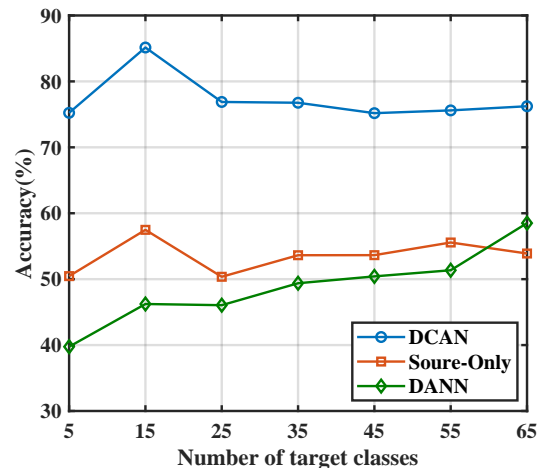


Fig. 9. The classification accuracy curve of different numbers of the target domain classes in the $C \rightarrow P$ task on Office-Home dataset.

ness of DCAN on UDA tasks when the category distribution of \mathcal{D}_s and \mathcal{D}_t are different.

7) *Time Complexity of DCAN*: To show the computational complexity of DCAN, we count the GPU time on four different tasks, i.e., $A \rightarrow W$, $D \rightarrow A$, $R \rightarrow C$ and $C \rightarrow P$. The time is cost by one epoch, and it is compared with that of two widely used methods DDC [14] and DANN [16]. All experiments are

TABLE VII
TRAINING TIME (S) OF DDC, DANN AND DCAN.

Method	A→W	D→A	R→C	C→P
DDC	10.99	7.86	55.99	53.44
DANN	10.46	7.41	53.88	51.61
DCAN	11.05	8.16	58.06	54.60

run on a device with an NVIDIA GTX1080Ti GPU. From the experiment results as shown in Table VII, we obtain the following observations: 1) The training time of DCAN and DDC is about 6% longer than DANN. The reason is that they both need to calculate the kernel matrix K . The computational complexity for calculating K is $O(n^2m)$, where n is the batch-size and m is the dimension of features. In practice, m is usually large, which makes it time-consuming to calculate K . 2) The training time of DANN is about 2% longer than that of DDC. This is because the CMMD term needs to calculate the inverse of K . The computational complexity of this step is $O(n^3)$. Fortunately, n is usually small in deep learning, which means that it does not take much time to calculate the inverse of K .

V. CONCLUSION

This paper presents a novel domain adaptation method, DCAN, to learn domain conditional-invariant features for image classification. DCAN introduces the CMMD metric to achieve conditional distribution alignment of the source and target domains. Since the marginal distribution alignment is not required, DCAN does not assume that the source and target domains share the same label distribution, thus it has wider application scenarios, such as Partial UDA. In addition, an extra mutual information is introduced to extract discriminant information from the target domain. DCAN is evaluated on four benchmark databases, and the results show that it achieves state-of-the-arts performance in both UDA and Partial UDA tasks.

How to introduce metric learning module to DCAN, and deal with more general problems such as HDA and zero-shot classification, are our future work.

REFERENCES

- [1] A. Krizhevsky, I. Sutskever, and G. E. Hinton, "Imagenet classification with deep convolutional neural networks," in *Advances in Neural Information Processing Systems*, 2012, pp. 1097–1105.
- [2] S. Ren, K. He, R. Girshick, and J. Sun, "Faster R-CNN: towards real-time object detection with region proposal networks," in *Advances in Neural Information Processing Systems*, 2015, pp. 91–95.
- [3] Y. Taigman, Y. Ming, M. Ranzato, and L. Wolf, "Deepface: Closing the gap to human-level performance in face verification," in *IEEE Conference on Computer Vision and Pattern Recognition*, 2014, pp. 1701–1708.
- [4] J. Donahue, Y. Jia, O. Vinyals, J. Hoffman, Z. Ning, E. Tzeng, and T. Darrell, "Decaf: a deep convolutional activation feature for generic visual recognition," in *International Conference on Machine Learning*, 2014, pp. 647–655.
- [5] J. Yosinski, J. Clune, Y. Bengio, and H. Lipson, "How transferable are features in deep neural networks?" in *Advances in Neural Information Processing Systems*, 2014, pp. 3320–3328.
- [6] M. Oquab, L. Bottou, I. Laptev, and J. Sivic, "Learning and transferring mid-level image representations using convolutional neural networks," in *IEEE Conference on Computer Vision and Pattern Recognition*, 2014, pp. 1717–1724.

- [7] S. J. Pan and Q. Yang, "A survey on transfer learning," *IEEE Transactions on Knowledge and Data Engineering*, vol. 22, no. 10, pp. 1345–1359, 2010.
- [8] K. Zhang, B. Schölkopf, K. Muandet, and Z. Wang, "Domain adaptation under target and conditional shift," in *International Conference on Machine Learning*, 2013, pp. 819–827.
- [9] J. Donahue, J. Hoffman, E. Rodner, K. Saenko, and T. Darrell, "Semi-supervised domain adaptation with instance constraints," in *IEEE Conference on Computer Vision and Pattern Recognition*, 2013, pp. 1–8.
- [10] C. X. Ren, D. Q. Dai, K. K. Huang, and Z. R. Lai, "Transfer learning of structured representation for face recognition," *IEEE Transactions on Image Processing*, vol. 23, no. 12, pp. 5440–5454, 2014.
- [11] P. Sinno Jialin, I. W. Tsang, J. T. Kwok, and Y. Qiang, "Domain adaptation via transfer component analysis," *IEEE Transactions on Neural Networks*, vol. 22, no. 2, pp. 199–210, 2011.
- [12] M. Long, J. Wang, G. Ding, J. Sun, and P. S. Yu, "Transfer feature learning with joint distribution adaptation," in *IEEE International Conference on Computer Vision*, 2014, pp. 2200–2207.
- [13] C. X. Ren, X. L. Xu, and H. Yan, "Generalized conditional domain adaptation: A causal perspective with low-rank translators," *IEEE Transactions on Cybernetics*, 2019, Accepted.
- [14] E. Tzeng, J. Hoffman, N. Zhang, K. Saenko, and T. Darrell, "Deep domain confusion: Maximizing for domain invariance," *arXiv preprint arXiv:1412.3474*, 2014.
- [15] M. Long, Y. Cao, J. Wang, and M. Jordan, "Learning transferable features with deep adaptation networks," in *International Conference on Machine Learning*, 2015, pp. 97–105.
- [16] Y. Ganin, E. Ustinova, H. Ajakan, P. Germain, H. Larochelle, F. Laviolette, M. Marchand, and V. Lempitsky, "Domain-adversarial training of neural networks," *Journal of Machine Learning Research*, vol. 17, pp. 2096–2030, 2016.
- [17] M. Long, J. Wang, and M. I. Jordan, "Unsupervised domain adaptation with residual transfer networks," in *Advances in Neural Information Processing Systems*, 2016, pp. 136–144.
- [18] M. Y. Liu and O. Tuzel, "Coupled generative adversarial networks," in *Advances in Neural Information Processing Systems*, 2016, pp. 469–477.
- [19] K. Bousmalis, N. Silberman, D. Dohan, D. Erhan, and D. Krishnan, "Unsupervised pixel-level domain adaptation with generative adversarial networks," in *IEEE Conference on Computer Vision and Pattern Recognition*, 2017, pp. 3722–3731.
- [20] J. Hoffman, E. Tzeng, T. Park, J. Y. Zhu, P. Isola, K. Saenko, A. A. Efros, and T. Darrell, "Cycada: Cycle-consistent adversarial domain adaptation," *arXiv preprint, arXiv:1711.03213*, 2017.
- [21] I. J. Goodfellow, J. Pouget-Abadie, M. Mirza, X. Bing, D. Warde-Farley, S. Ozair, A. Courville, and Y. Bengio, "Generative adversarial nets," in *Advances in Neural Information Processing Systems*, 2014, pp. 2672–2680.
- [22] A. Gretton, K. M. Borgwardt, M. Rasch, B. Schölkopf, and A. Smola, "A kernel two-sample test," *Journal of Machine Learning Research*, vol. 13, pp. 723–773, 2012.
- [23] E. Tzeng, J. Hoffman, K. Saenko, and T. Darrell, "Adversarial discriminative domain adaptation," in *IEEE Conference on Computer Vision and Pattern Recognition*, 2017, pp. 7167–7176.
- [24] R. Xu, G. Li, J. Yang, and L. Lin, "Unsupervised domain adaptation: An adaptive feature norm approach," *arXiv preprint arXiv:1811.07456*, 2018.
- [25] H. Yan, Y. Ding, P. Li, Q. Wang, Y. Xu, and W. Zuo, "Mind the class weight bias: Weighted maximum mean discrepancy for unsupervised domain adaptation," in *IEEE Conference on Computer Vision and Pattern Recognition*, 2017, pp. 2272–2281.
- [26] Z. Cao, M. Long, J. Wang, and M. I. Jordan, "Partial transfer learning with selective adversarial networks," in *IEEE Conference on Computer Vision and Pattern Recognition*, 2018, pp. 2724–2732.
- [27] Z. Cao, L. Ma, M. Long, and J. Wang, "Partial adversarial domain adaptation," in *European Conference on Computer Vision*, 2018, pp. 135–150.
- [28] A. Smola, A. Gretton, L. Song, and B. Schölkopf, "A Hilbert space embedding for distributions," in *International Conference on Algorithmic Learning Theory*. Springer, 2007, pp. 13–31.
- [29] Y. Ren, J. Li, Y. Luo, and J. Zhu, "Conditional generative moment-matching networks," in *Advances in Neural Information Processing Systems*, 2016, pp. 2928–2936.
- [30] M. Long, H. Zhu, J. Wang, and M. I. Jordan, "Deep transfer learning with joint adaptation networks," in *International Conference on Machine Learning*, 2017, pp. 2208–2217.

- [31] J. Wang, Y. Chen, S. Hao, W. Feng, and Z. Shen, “Balanced distribution adaptation for transfer learning,” in IEEE International Conference on Data Mining, 2017, pp. 1129–1134.
- [32] M. Long, Z. Cao, J. Wang, and M. I. Jordan, “Conditional adversarial domain adaptation,” in Advances in Neural Information Processing Systems, 2018, pp. 1647–1657.
- [33] S. Mehrkanoon and J. A. Suykens, “Regularized semipaired kernel cca for domain adaptation,” IEEE Transactions on Neural Networks and Learning Systems, vol. 29, no. 7, pp. 3199–3213, 2018.
- [34] S. Mehrkanoon, “Cross-domain neural-kernel networks,” Pattern Recognition Letters, vol. 125, pp. 474–480, 2019.
- [35] J. Zhang, Z. Ding, W. Li, and P. Ogunbona, “Importance weighted adversarial nets for partial domain adaptation,” in IEEE Conference on Computer Vision and Pattern Recognition, 2018, pp. 8156–8164.
- [36] L. Song, J. Huang, A. Smola, and K. Fukumizu, “Hilbert space embeddings of conditional distributions with applications to dynamical systems,” in International Conference on Machine Learning, 2009, pp. 961–968.
- [37] C. R. Baker, “Joint measures and cross-covariance operators,” Transactions of the American Mathematical Society, vol. 186, pp. 273–289, 1973.
- [38] O. Sener, H. O. Song, A. Saxena, and S. Savarese, “Learning transferrable representations for unsupervised domain adaptation,” in Advances in Neural Information Processing Systems, 2016, pp. 2110–2118.
- [39] L. Hu, M. Kan, S. Shan, and X. Chen, “Duplex generative adversarial network for unsupervised domain adaptation,” in IEEE Conference on Computer Vision and Pattern Recognition, 2018, pp. 1498–1507.
- [40] Y. LeCun, L. Bottou, Y. Bengio, P. Haffner et al., “Gradient-based learning applied to document recognition,” Proceedings of the IEEE, vol. 86, no. 11, pp. 2278–2324, 1998.
- [41] J. S. Denker, W. R. Gardner, H. P. Graf, D. Henderson, R. E. Howard, W. E. Hubbard, L. D. Jackel, H. S. Baird, and I. Guyon, “Neural network recognizer for hand-written zip code digits,” in Advances in Neural Information Processing Systems, 1988, pp. 323–331.
- [42] Y. Netzer, T. Wang, A. Coates, A. Bissacco, B. Wu, and A. Y. Ng, “Reading digits in natural images with unsupervised feature learning,” in Advances in Neural Information Processing Systems Workshop, 2011.
- [43] K. Saenko, B. Kulis, M. Fritz, and T. Darrell, “Adapting visual category models to new domains,” in European Conference on Computer Vision, 2010, pp. 213–226.
- [44] H. Venkateswara, J. Eusebio, S. Chakraborty, and S. Panchanathan, “Deep hashing network for unsupervised domain adaptation,” in IEEE Conference on Computer Vision and Pattern Recognition, 2017, pp. 5018–5027.
- [45] K. He, X. Zhang, S. Ren, and J. Sun, “Deep residual learning for image recognition,” in IEEE Conference on Computer Vision and Pattern Recognition, 2016, pp. 770–778.
- [46] D. P. Kingma and J. Ba, “Adam: A method for stochastic optimization,” arXiv preprint, arXiv:1412.6980, 2014.
- [47] M. Ghifary, W. B. Kleijn, M. Zhang, D. Balduzzi, and L. Wen, “Deep reconstruction-classification networks for unsupervised domain adaptation,” in European Conference on Computer Vision, 2016, pp. 597–613.
- [48] S. Sankaranarayanan, Y. Balaji, C. D. Castillo, and R. Chellappa, “Generate to adapt: Aligning domains using generative adversarial networks,” in IEEE Conference on Computer Vision and Pattern Recognition, 2018, pp. 8503–8512.
- [49] T. Matsuura, K. Saito, and T. Harada, “Twins: Two weighted inconsistency-reduced networks for partial domain adaptation,” arXiv preprint, arXiv:1812.07405, 2018.
- [50] L. V. D. Maaten and G. Hinton, “Visualizing data using t-SNE,” Journal of Machine Learning Research, vol. 9, pp. 2579–2605, 2008.